Overdamped Brownian dynamics in piecewise-defined energy landscapes

Thomas H. Gray [1,2] and Ee Hou Yong [3,*]

[1] *Statistical Physics Group, Department of Chemical Engineering and Biotechnology, West Cambridge Site, Philippa Fawcett Drive, University of Cambridge, CB3 0AS, Cambridge, United Kingdom*

[2] *T.C.M. Group, Cavendish Laboratory, JJ Thomson Avenue, Cambridge CB3 0HE, United Kingdom*

[3] *School of Physical and Mathematical Sciences, Nanyang Technological University, Singapore 637371, Singapore*

(Received 24 December 2018; revised manuscript received 14 October 2019; accepted 17 April 2020; published 18 May 2020; corrected 28 August 2020)

We study the overdamped Brownian dynamics of particles moving in piecewise-defined potential energy landscapes $U(x)$, where the height Q of each section is obtained from the exponential distribution $p(Q) = a\beta\exp(-a\beta Q)$, where β is the reciprocal thermal energy, and $a > 0$. The *averaged* effective diffusion coefficient $\langle D_{\text{eff}}\rangle$ is introduced to characterize the diffusive motion: $\langle x^2\rangle = 2\langle D_{\text{eff}}\rangle t$. A general expression for $\langle D_{\text{eff}}\rangle$ in terms of $U(x)$ and $p(Q)$ is derived and then applied to three types of energy landscape: flat sections, smooth maxima, and sharp maxima. All three cases display a transition between subdiffusive and diffusive behavior at $a = 1$, and a reduction to free diffusion as $a \to \infty$. The behavior of $\langle D_{\text{eff}}\rangle$ around the transition is investigated and found to depend heavily upon the shape of the maxima: Energy landscapes made up of flat sections or smooth maxima display power-law behavior, while for landscapes with sharp maxima, strongly divergent behavior is observed. Two aspects of the subdiffusive regime are studied: the growth of the mean squared displacement with time and the distribution of mean first-passage times. For the former, agreement between Brownian dynamics simulations and a coarse-grained equivalent was observed, but the results deviated from the random barrier model's predictions. The discrepancy could be a finite-time effect. For the latter, agreement between the characteristic exponent calculated numerically and that predicted by the random barrier model is observed in the large-amplitude limit.

DOI: 10.1103/PhysRevE.101.052123

I. INTRODUCTION

It is well known that the mean squared displacement of an ensemble of freely diffusing, overdamped, Brownian particles grows according to $\langle x^2\rangle = 2D_{\text{free}}t$, where D_{free} denotes the free diffusion coefficient, which is equal to $k_{\text{B}}T/\gamma$: the ratio of the thermal energy to the damping coefficient. Since this result was established and publicized by both Einstein [1] and Smoluchowski [2], many studies of diffusion have been performed. A wide range of phenomena, categorizable as diffusive, subdiffusive, or superdiffusive depending upon how the mean squared displacement grows with time, are found. Diffusive and subdiffusive behavior has been observed in a variety of biological systems, with some displaying a transition between the two. For instance, increasing the spatial density of obstacles placed upon a lattice on which a colloid moves can bring about a transition from diffusive to subdiffusive behavior [3]. Other systems exhibit the reverse of this transition over time, where the timescale is determined by, for example, the spatial density of solid phase domains in lipid bilayers [4] and many-body volume-exclusion effects upon the motion of water molecules on the surface of proteins [5]. There, a heavy-tailed distribution of waiting times for jumps from one trapping site to another is believed to be the cause of the initially subdiffusive behavior.

Turning now to systems with a periodic background, we again find transitions over time from subdiffusion to diffusion. This is well illustrated by the motion of colloids over a substrate with quasicrystalline-patterned holes [6,7]. In fact, the transition has two stages: from free diffusion to subdiffusion and then to diffusion at a reduced rate. This reflects the existence of multiple timescales: The first to feel the confining nature of the minima; the second to begin to move between minima [8,9].

Random potential-energy landscapes, where the energy of each lattice site—or barrier height between sites—is taken from an exponential probability distribution, give rise to the possibility of new phenomena. In addition to the aforementioned transitions over time [10,11] is the possibility of an enduring subdiffusive regime brought about by a change in the parameter controlling the shape of the exponential distribution [12–17]. We seek to study the diffusive regime, and the transition to the subdiffusive regime, for piecewise-defined energy landscapes composed of flat sections, smooth maxima, and sharp maxima.

The long-time motion in sinusoidal potential energy landscapes is diffusive with an *effective* diffusion coefficient D_{eff}, where $D_{\text{eff}} \leqslant D_{\text{free}}$ [8,18]. Lifson and Jackson derived a general expression for D_{eff} applicable in one dimension [19]. (Jackson and Coriell later built upon this work in an effort to extend the results into two and three dimensions [20]). Zwanzig extended Lifson and Jackson's work by proposing a framework to study the overdamped Brownian dynamics of systems where the potential energy landscape comprises a rough component superimposed onto a smooth background [21]. Both Zwanzig and Lifson and Jackson used a mean first-passage time formalism to derive their results (see, e.g., Ref. [22]), and it is upon this formalism that our work is based.

*Corresponding author: eehou@ntu.edu.sg

To illustrate his work, Zwanzig calculated the effective diffusion coefficient for two energy landscapes: a sinusoid and a surface characterized by Gaussian-distributed roughness. In the second case, a very strong thermal energy dependence was discovered: $D_{\text{eff}} = D_{\text{free}}/\mathrm{e}^{(\beta\varepsilon)^2}$, where ε is the root-mean-squared roughness and $\beta = 1/k_{\text{B}}T$. Banerjee *et al.* built upon Zwanzig's work by calculating this same diffusion coefficient, but without resorting to the spatial averaging which Zwanzig used [23]. By doing so, they avoided the oversmoothing of the energy landscape, and hence the loss of the suppressing effect of the rare, ultratall barriers (the equivalent of what Banerjee *et al.* term "three site traps") on the rate of diffusion. Instead, by considering a discrete Gaussian lattice and summing over the transition rates between individual sites, Banerjee *et al.* calculated an exact expression for the mean first-passage time, and hence the effective diffusion coefficient. Chief among their findings is an enhanced (relative to Zwanzig's result) suppression of diffusive motion for all nonzero ε: a feature confirmed by simulation results presented in the same paper.

We aim to build upon the work of Banerjee *et al.* by studying overdamped Brownian motion in one-dimensional, piecewise-defined energy landscapes, where the barrier heights $\{Q_i\}$ are taken from the exponential distribution $p(Q) = a\beta\exp(-a\beta Q)$, and $a > 0$ is a constant. In addition to flat sections, we will also study a range of symmetric barrier shapes (the asymmetric case will be studied briefly).

To characterize the motion, we will work with *averaged* mean first-passage times $\langle\tau\rangle$, and *averaged* effective diffusion coefficients $\langle D_{\text{eff}}\rangle$, where the angled brackets denote averages over the probability distribution $p(Q)$.

A transition between subdiffusive and diffusive behavior is observed at $a = 1$ for all energy landscapes considered. The existence of this transition is concordant with the findings of Bouchaud and others [14–16,24,25]. Writing $a = 1 + \delta$ (where δ is small and positive) in the expression for $\langle D_{\text{eff}}\rangle$ facilitates study of the nature of the transition. Energy landscapes with smooth barriers exhibit power-law behavior $\langle D_{\text{eff}}\rangle \propto \delta^{\eta}$, where η is determined by the order of the first nonvanishing spatial derivative of the energy landscape evaluated at its maxima. In stark contrast, landscapes with sharp barriers give rise to significantly stronger dependencies.

In the next section, we will derive a general expression for the averaged effective diffusion coefficient by considering the mean first-passage time from one end of the energy landscape $U(x)$ to the other. Thereafter, we turn to study three distinct cases: case 1, energy landscapes composed of flat sections; case 2, energy landscapes with smooth barriers; and case 3, energy landscapes with sharp barriers. Case 1 will be seen to be a limiting form of case 2, and both are distinct from case 3. The results of Brownian dynamics simulations performed for cases 2 and 3 are presented in the relevant sections.

We conclude by discussing the subdiffusive regime corresponding to $a < 1$. Some agreement between the random barrier model's predictions and simulations of both the mean squared displacement and the distribution of mean first-passage times is observed; the discrepancy is believed to be a consequence of differing expressions for the mean first-passage time. Note that by writing $a = \beta_g/\beta = T/T_g$, where T_g is the glass-transition temperature, the connection to glassy system can be made explicit [15].

II. DERIVING $\langle D_{\text{eff}}\rangle$

Consider a continuous, piecewise-defined potential energy landscape $U(x)$ made up of sections of width L and with a repeat unit of N sections. Each section is symmetric about the single, central maximum, and starts and finishes at the same potential. For finite values of N, the effective diffusion coefficient is given by the Lifson-Jackson expression

$$D_{\text{eff}} = \frac{D_{\text{free}}}{\langle e^{\beta U}\rangle_{\text{x}}\langle e^{-\beta U}\rangle_{\text{x}}}, \tag{1}$$

where $\langle\rangle_{\text{x}}$ denotes the spatial average [19]. Each particle's motion in this type of potential energy landscape consists of relatively long periods of time spent around the confining minima interspersed by relatively short transitions between adjacent minima. This is reminiscent of diffusion on regular lattices. Derrida, and others, give the effective diffusion coefficient, up to a factor of the lattice constant squared, as

$$D_{\text{eff}} = \frac{N}{\sum_{n=1}^{N}\frac{1}{W_{n+1,n}}}, \tag{2}$$

where $W_{n+1,n}$ is the transition rate from site n to site $n+1$ [26–28]. When the amplitude of each maximum is distributed according to some distribution $\rho(W)$, the expression for the *averaged* effective diffusion coefficient in the thermodynamic limit $N \to \infty$ is

$$\langle D_{\text{eff}}\rangle = \left\langle\frac{1}{W}\right\rangle^{-1}, \tag{3}$$

where $\langle\rangle$ denotes the disorder average [26].

Building upon work carried out by Kalnin and Berezhkovskii [29], we will demonstrate equivalence between Eqs. (1) and (2). Having established the link, we will use (3) to derive an expression for the averaged effective diffusion coefficient in terms of an averaged mean first-passage time and ultimately as a function of disorder and spatial averages over the energy landscape.

Equation (2) assumes that forward and backward transition rates between two lattice sites are equal, i.e., $W_{n+1,n} = W_{n,n+1}$. (For potential energy landscapes, this means that all of the minima lie at the same potential energy.) This allows us to rewrite Eq. (2) as follows,

$$\frac{1}{D_{\text{eff}}} = \frac{1}{2N}\sum_{i=1}^{N}\left(\frac{1}{W_{n+1,n}} + \frac{1}{W_{n-1,n}}\right), \tag{4}$$

where we have chosen the indices on the second term so that both transition rates in the sum refer to the same starting site: The first is for a jump in the positive direction, while the second is for a jump in the negative direction. By identifying the mean first-passage time τ_n from site n to either of sites $n-1$ and $n+1$ as the reciprocal of the sum of the transition rates (i.e., $1/\tau_n = W_{n+1,n} + W_{n-1,n}$), and the probabilities of jumping to the left $\mathcal{P}^{-}_{L,n}$ and to the right $\mathcal{P}^{+}_{R,n}$ as $W_{n-1,n}/\tau_n$ and $W_{n+1,n}/\tau_n$, respectively, we may rewrite Eq. (4) as

$$\frac{1}{D_{\text{eff}}} = \frac{1}{N}\sum_{i=1}^{N}\frac{1}{\frac{\tau_n}{\mathcal{P}^{+}_{R,n}\mathcal{P}^{-}_{L,n}}}. \tag{5}$$

This is a useful expression because the transition rates have been replaced by jump probabilities and mean first-passage times, which, for continuous potential energy landscapes, are easy to calculate.

Equation (1) gives the effective diffusion coefficient in terms of spatial averages over the (exponential of) the potential energy landscape. What is the physical equivalent of this spatial averaging? It is the ensemble of particles exploring the potential energy landscape. More specifically, it is the ensemble diffusing over a distance greater than the length of the repeat unit. Only beyond this stage in the motion will the diffusive behavior be described by the Lifson-Jackson expression for D_{eff}. This sets characteristic length- and timescales for the motion: NL and the time taken for a *sufficient* fraction of the ensemble to travel a distance of NL, respectively.

Once this stage of the motion has been entered into, the relevant lengthscale is NL, which means that the focus is upon the time taken for a particle to move from one site to its identical counterpart in either of the adjacent repeat units. Look now to Eq. (2), the Derrida expression for the effective diffusion coefficient. Once the effective diffusion regime has been entered into, it no longer makes sense to characterize the motion in terms of transitions between lattice sites within the same repeat unit. Rather, considering transitions between equivalent sites in adjacent repeat units is more appropriate. This means that Eq. (2) becomes

$$\frac{1}{D_{\text{eff}}} = \frac{1}{\frac{\tau}{2\mathcal{P}_R\mathcal{P}_L}}, \tag{6}$$

where τ is the mean first-passage time from a site in one repeat unit to the same site in either of the two adjacent repeat units, and $\mathcal{P}_R$ and $\mathcal{P}_L$ are the probabilities that a particle makes the above transition to the right and left, respectively. For a particle starting from $x = 0$ in an energy landscape with a repeat length of NL, the probabilities are [22]

$$\mathcal{P}_R = 1 - \mathcal{P}_L = \frac{\int_0^{NL} dy\, e^{\beta U(y)}}{\int_{-NL}^{NL} dy\, e^{\beta U(y)}}. \tag{7}$$

Because of periodicity, we can rewrite the integral currently defined over the range $[-NL, NL]$ as an integral over the range $[0, NL]$: $\int_{-NL}^{0} dy\, e^{\beta U(y)} = \int_0^{NL} dy\, e^{\beta U(y)}$. Doing so, we find that $\mathcal{P}_R = \mathcal{P}_L = \frac{1}{2}$.

The mean first-passage time is [22]

$$\tau = \frac{\mathcal{P}_R}{D_{\text{free}}} \int_0^{NL} dy\, e^{\beta U(y)} \int_{-NL}^{y} dz\, e^{-\beta U(z)} - \frac{\mathcal{P}_L}{D_{\text{free}}} \int_{-NL}^{0} dy\, e^{\beta U(y)} \int_{-NL}^{y} dz\, e^{-\beta U(z)}. \tag{8}$$

Separating the first integral into two—one where the inner integral runs over the range $[-NL, 0]$ and one where the inner integral runs over the range $[0, y]$—and inserting the expressions for $\mathcal{P}_{R,L}$, we obtain

$$\tau = \frac{1}{2D_{\text{free}}} \int_0^{NL} dy\, e^{\beta U(y)} \int_{-NL}^{0} dz\, e^{-\beta U(z)} + \frac{1}{2D_{\text{free}}} \int_0^{NL} dy\, e^{\beta U(y)} \int_0^{y} dz\, e^{-\beta U(z)} - \frac{1}{2D_{\text{free}}} \int_{-NL}^{0} dy\, e^{\beta U(y)} \int_{-NL}^{y} dz\, e^{-\beta U(z)}. \tag{9}$$

As a result of periodicity, the third double integral in Eq. (9) can be rewritten over the range $[0, NL]$, and so cancels with the second double integral. The mean first-passage time is thus

$$\tau = \frac{1}{2D_{\text{free}}} \int_0^{NL} dy\, e^{\beta U(y)} \int_{-NL}^{0} dz\, e^{-\beta U(z)}. \tag{10}$$

Using periodicity, we rewrite the second of the two integrals in Eq. (10) over the same range as the first. Recasting each of them as a spatial average, we find

$$\tau = \frac{(NL)^2}{2D_{\text{free}}} \langle e^{\beta U} \rangle_{\text{x}} \langle e^{-\beta U} \rangle_{\text{x}}. \tag{11}$$

Inserting Eq. (11) into Eq. (6), and recalling that $\mathcal{P}_R = \mathcal{P}_L = \frac{1}{2}$, we find

$$D_{\text{eff}} = \frac{D_{\text{free}}}{(NL)^2 \langle \text{e}^{\beta U} \rangle_{\text{x}} \langle \text{e}^{-\beta U} \rangle_{\text{x}}}. \tag{12}$$

Finally, rescaling by the lattice constant (now NL) squared [28], we find

$$D_{\text{eff}} = \frac{D_{\text{free}}}{\langle e^{\beta U} \rangle_{\text{x}} \langle e^{-\beta U} \rangle_{\text{x}}}, \tag{13}$$

which is the same as Eq. (1), the Lifson-Jackson expression for the effective diffusion coefficient [19].

Having demonstrated equivalence between Eqs. (1) and (2), we will proceed to use Eq. (3) to derive the *averaged* effective diffusion coefficient.

Following the reasoning laid out above, we write

$$\left\langle \frac{1}{W} \right\rangle = \left\langle \frac{1}{W^+} \right\rangle = \frac{1}{2} \left\langle \frac{1}{W^+} + \frac{1}{W^-} \right\rangle = \left\langle \frac{W^+ + W^-}{2W^+W^-} \right\rangle, \tag{14}$$

where we relabeled W to W^+ to make clear that the disorder average is being taken over a transition rate in the positive direction (the symmetry of transition rates between adjacent sites allows us to do this). Then, to construct the equivalent of Eq. (4), we introduced a transition rate (from the same lattice site) in the negative direction. Replacing the transition rates by the mean first-passage time and jump probabilities, we find

$$\left\langle \frac{1}{W} \right\rangle = \frac{1}{2} \left\langle \frac{\tau}{\mathcal{P}_R\mathcal{P}_L} \right\rangle = 2\langle \tau \rangle, \tag{15}$$

where the last equality follows because we are considering motion from one lattice site to either of the equivalent sites in the immediately adjacent repeat units.

Using this result in Eq. (3) and rescaling by the lattice constant (NL) squared, we find the following expression for the averaged effective diffusion coefficient:

$$\langle D_{\text{eff}} \rangle = \lim_{N \to \infty} \frac{(NL)^2}{2\langle \tau_N \rangle}, \tag{16}$$

where we have relabeled τ to τ_N to emphasize that we are considering the mean first-passage time from one site to either of the equivalent sites a distance of NL away.

We can rewrite Eq. (10) in a form more amenable to the calculation of the disorder average:

$$\tau_N = \frac{1}{2D_{\text{free}}} \sum_{i=1}^{N} \int_0^L dy\, e^{\beta U_i} \int_0^L dz\, e^{-\beta U_i} + \frac{1}{2D_{\text{free}}} \sum_{i \neq j} \int_0^L dy\, e^{\beta U_i} \int_0^L dz\, e^{-\beta U_j}, \quad (17)$$

where, thanks to the underlying form of the potential energy landscape being the same in each and every section, we are able to cast all of the integrals over the same range. The averaged mean first-passage time is

$$\langle \tau_N \rangle = \int dQ_1 \ldots dQ_N\, \tau_N(Q_1, \ldots, Q_N) p(Q_1, \ldots, Q_N), \quad (18)$$

where p is the joint probability distribution. Since the amplitudes are chosen independently of one another, $p(Q_1, \cdots, Q_N)$ becomes the product of N individual probability distributions $p(Q_1) \ldots p(Q_N)$. Inserting Eq. (17) into Eq. (18), we find

$$\langle \tau_N \rangle = \frac{NL^2}{2D_{\text{free}}} \int dQ_1\, \langle e^{\beta U_1} \rangle_{\text{x}} \langle e^{-\beta U_1} \rangle_{\text{x}} + \frac{N(N-1)L^2}{2D_{\text{free}}} \times \int dQ_1 dQ_2\, \langle e^{\beta U_1} \rangle_{\text{x}}\, p(Q_1) \langle e^{-\beta U_2} \rangle_{\text{x}}\, p(Q_2). \quad (19)$$

Finally, inserting Eq. (19) into Eq. (16), we obtain

$$\langle D_{\text{eff}} \rangle = \frac{D_{\text{free}}}{\int dQ_1 \langle e^{\beta U_1} \rangle_{\text{x}}\, p(Q_1) \int dQ_2 \langle e^{-\beta U_2} \rangle_{\text{x}}\, p(Q_2)}. \quad (20)$$

Note that the spatial averages are taken over *individual* sections of the energy landscape, not *multiple* sections as per Zwanzig's approach. This is important for reasons given in Ref. [23] and described in the introduction.

III. CASE 1: FLAT SECTIONS

We begin by considering the simplest nontrivial energy landscape: one composed of flat sections. The ith section ($i = 1, 2, ..., N$) of the energy landscape is defined over the range $[(i-1)L, iL]$ and given by $U_i(x) = Q_i$. An example is shown in Fig. 1. The spatial averages in Eq. (20) are as follows:

$$\langle e^{\beta U_1} \rangle_{\text{x}} = \frac{1}{L} \int_0^L ex\, e^{\beta Q_1} = e^{\beta Q_1}, \quad (21)$$

$$\langle e^{-\beta U_2} \rangle_{\text{x}} = e^{-\beta Q_2}. \quad (22)$$

Inserting these expressions and the probability distribution $p(Q) = a\beta \exp(-a\beta Q)$ into Eq. (20), and relabelling $\beta Q_{1,2} = x, y$, respectively, we find

$$\langle D_{\text{eff}} \rangle_{\text{F}} = \frac{1}{a^2} \frac{D_{\text{eff}}}{\int_0^\infty dx\, e^{-(a-1)x} \int_0^\infty dy\, e^{-(a+1)y}}, \quad (23)$$

where the subscript F denotes the case of "flat sections."

While the second integral always converges ($a > 0$), the first does not: For values of $a \leqslant 1$ it is unbounded, thereby predicting nondiffusive behavior. However, for $a > 1$, it is finite, and the averaged effective diffusion coefficient is nonzero. This is the first manifestation of the transition between—as we will come to see—diffusive and subdiffusive behavior. For the sake of brevity, we will not perform this analysis of divergence and convergence for every energy landscape considered. One can show that the result is always the same: a transition at $a = 1$. The behavior for $a \leqslant 1$ will be discussed later. Evaluating the integrals in Eq. (23), we obtain

$$\langle D_{\text{eff}} \rangle_{\text{F}} = \left(1 - \frac{1}{a^2}\right) D_{\text{free}}. \quad (24)$$

We will now examine the behavior of $\langle D_{\text{eff}} \rangle_{\text{F}}$ in two limits. First, as a increases, the probability distribution $p(Q)$ becomes ever more skewed toward smaller values of Q. We expect, therefore, to return to free diffusion as $a \to \infty$. Second, $a \to 1^+$ looks at the behavior around the transition.

From Eq. (24), it is immediately clear that $\lim_{a\to 0} \langle D_{\text{eff}} \rangle_{\text{F}} = D_{\text{free}}$, as expected. By writing $a = 1 + \delta$, and examining the limit $\delta \to 0$, the second limit can be studied:

$$\langle D_{\text{eff}}(a = 1 + \delta) \rangle_{\text{F}} = \frac{\delta(2+\delta)}{(1+\delta)^2} D_{\text{free}}, \quad (25)$$

$$\Rightarrow \langle D_{\text{eff}}(a = 1 + \delta) \rangle_{\text{F}} \sim \delta \text{ as } \delta \to 0^+. \quad (26)$$

Around the transition, the averaged effective diffusion coefficient grows linearly with a.

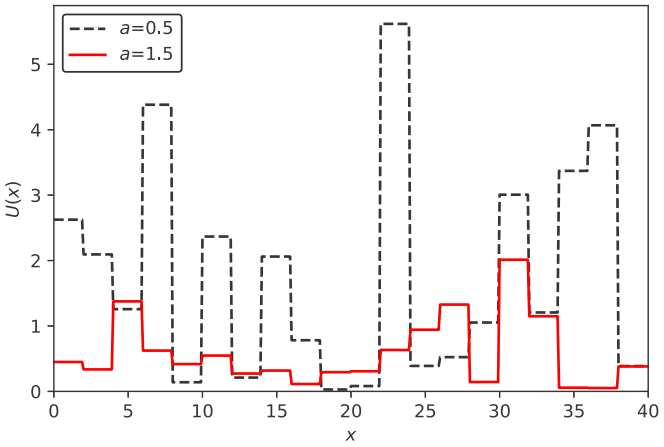

FIG. 1. Example energy landscapes composed of flat sections. The black (dashed) and red (solid) lines correspond to $a = 0.5$ and $a = 1.5$, respectively ($L = 2$).

IV. CASE 2: SMOOTH MAXIMA

We will study two types of potential energy landscape with symmetric maxima: power law and cosine forms. The behavior of the averaged effective diffusion coefficient around the transition is studied, and the connection between this behavior and the energy landscape's curvature is drawn. Finally, we generalise our result and consider the case of asymmetric maxima.

A. Power law forms

The ith section ($i = 1, 2, ..., N$) of the potential energy landscape is defined over the range $[(i-1)L, iL]$. An exponent m characterizes the shape of the energy landscape. For

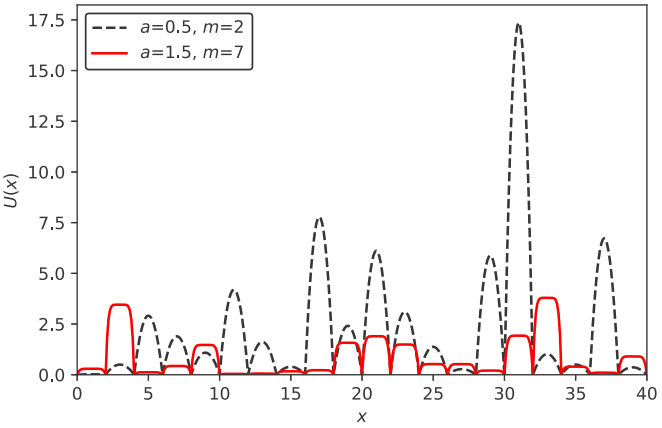

FIG. 2. Example energy landscapes with smooth maxima: the black (dashed) and red (solid) lines correspond to $a = 0.5$, $m = 2$ and $a = 1.5$, $m = 7$, respectively ($L = 2$).

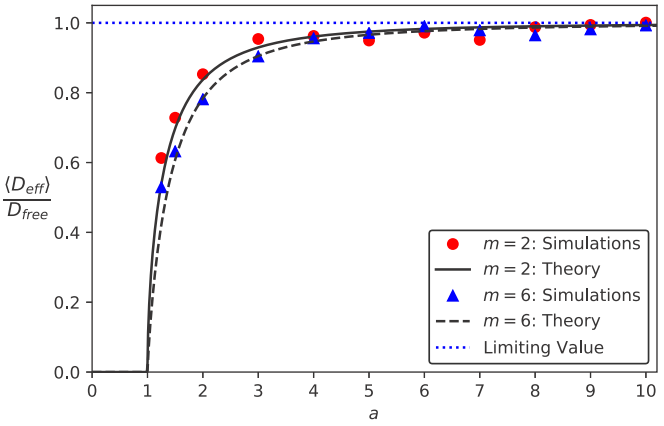

FIG. 3. The results of Brownian dynamics simulations (red circles and blue triangles) are presented alongside the theoretical predictions (solid and dashed lines) for two "smooth" energy landscapes characterized by $m = 2$ and $m = 6$, respectively.

even values of m, the energy landscape is given by

$$U_i(x) = Q_i\left[1 - \left(\frac{2x}{L} - (2i-1)\right)^m\right], \tag{27}$$

while for odd values of m, this expression describes the second half of the ith section: $[(i-\frac{1}{2})L, iL]$ (i.e., from $U = Q_i$ to $U = 0$); the other half is the mirror image in the line $x = (i-\frac{1}{2})L$. An example is shown in Fig. 2.

For the purposes of this calculation, we will assume that m is even. However, the final result also holds when m is odd: The only difference in the calculation is in the first line, where, instead of integrating from 0 to L, we would integrate from $L/2$ to L and double the result. The spatial average is

$$\langle e^{\beta U_1}\rangle_{\rm x} = \frac{e^{\beta Q_1}}{L}\int_0^L dx\, e^{-\beta Q_1\left(\frac{2x}{L}-1\right)^m}. \tag{28}$$

Hence, the first of the two integrals in Eq. (20)– -the expression for the averaged effective diffusion coefficient—is

$$a\beta\int_0^\infty dQ_1 \frac{e^{\beta Q_1}}{L}\int_0^L dx\, e^{-\beta Q_1\left(\frac{2x}{L}-1\right)^m} e^{-a\beta Q_1}. \tag{29}$$

Swapping the order of integration, and changing variables to $u = \frac{2x}{L} - 1$, we obtain

$$\int dQ_1 \langle e^{\beta U_1}\rangle_{\rm x}\, p(Q_1) = a\int_0^1 du \frac{1}{a-1+u^m}. \tag{30}$$

Correspondingly, the second integral is

$$\int dQ_2 \langle e^{-\beta U_2}\rangle_{\rm x}\, p(Q_2) = a\int_0^1 du \frac{1}{a+1-u^m}. \tag{31}$$

The averaged effective diffusion coefficient is thus

$$\langle D_{\rm eff}\rangle_{\rm Sm,P} = \frac{D_{\rm free}}{a^2\int_0^1 du\frac{1}{a-1+u^m}\int_0^1 dv\frac{1}{a+1-v^m}}, \tag{32}$$

where the subscript Sm,P denotes the case of "smooth maxima: power law forms." Both of these integrals can be written in terms of a hypergeometric function:

$$\langle D_{\rm eff}\rangle_{\rm Sm,P} = \frac{\left(1-\frac{1}{a^2}\right)D_{\rm free}}{{}_2F_1\left(\frac{1}{m},1;\frac{m+1}{m};\frac{-1}{a-1}\right){}_2F_1\left(\frac{1}{m},1;\frac{m+1}{m};\frac{1}{a+1}\right)}. \tag{33}$$

Brownian dynamics simulations to test the above were performed as follows: For a given value of m, an energy landscape stretching from $x = 0$ to $x = 20L$ (i.e., 20 maxima) was constructed by sampling the exponential distribution of barrier heights. Reflecting and absorbing boundary conditions were imposed at $x = 0$ and $x = 20L$, respectively, and a particle initialized at $x = 0$. With $k_{\rm B}T = \gamma = 1$, the overdamped Brownian motion was simulated until the particle reached the absorbing boundary; the time taken—the first-passage time—was recorded. A new set of amplitudes was then generated and the above procedure was repeated. First-passage times were recorded for $\mathcal{O}(10^3$–$10^4)$ energy landscapes and the averaged mean first-passage time was calculated. Finally, Eq. (16) was used to calculate the averaged effective diffusion coefficient. Note that the expression for $\langle D_{\rm eff}\rangle$ obtained from Eq. (16) when we impose one reflecting and one absorbing boundary (as in the simulations) is unchanged compared to the case of two absorbing boundaries, for which we derived the result.

Figure 3 shows the simulation results and theoretical prediction for power law energy landscapes with smooth maxima characterized by $m = 2$ and $m = 6$. Good agreement is observed.

Before we study the properties of the averaged effective diffusion coefficient, let us draw the connection between cases 1 and 2. Increasing the value of m flattens out the maxima, as shown in Fig. 2. Thus, as $m \to \infty$, the maxima becomes flat, exactly as in case 1. Evaluating Eq. (33) in this limit, we find

$$\lim_{m\to\infty}\langle D_{\rm eff}\rangle_{\rm Sm,P} = \frac{\left(1-\frac{1}{a^2}\right)D_{\rm free}}{{}_2F_1\left(0,1;1;\frac{-1}{a-1}\right){}_2F_1\left(0,1;1;\frac{1}{a+1}\right)},$$
$$= \left(1-\frac{1}{a^2}\right)D_{\rm free}, \tag{34}$$

where we have made use of standard properties of the hypergeometric function [30]. This is identical to Eq. (24)–the averaged effective diffusion coefficient for an energy landscape composed of flat sections. Case 1 can thus be viewed as a limiting form of case 2.

By noting that $\lim_{x\to 0^\pm}{}_2F_1(p,q;r,x) = 1$ [30], the reduction to free diffusion as $a \to \infty$ in case 2 [Eq. (33)] follows

simply. Looking to the second limit, we investigate the hypergeometric functions in turn. First,

$$ {}_2F_1\left(\frac{1}{m}, 1; \frac{m+1}{m}; \frac{1}{2+\delta}\right) = \sum_{k=0}^{\infty} \frac{\left(\frac{1}{m}\right)_k (1)_k}{2^k \left(\frac{1+m}{m}\right)_k k!} \left(1+\frac{\delta}{2}\right)^{-k}. \tag{35} $$

As $\delta \to 0^+$, we obtain

$$ {}_2F_1\left(\frac{1}{m}, 1; \frac{m+1}{m}; \frac{1}{2+\delta}\right) \sim \mathcal{C}_0 + \mathcal{C}_1\delta + \cdots, \tag{36} $$

where the $\{\mathcal{C}_i\}$ are constants. For our purposes, the most important feature of this expansion is $\mathcal{C}_0 \neq 0$, because it means that this hypergeometric function makes no contribution to the leading-order term in δ. Hence, we turn our attention to the other hypergeometric function: ${}_2F_1(\frac{1}{m}, 1; \frac{m+1}{m}, \frac{-1}{\delta})$, which can be written as [30]

$$ \delta^1 \left[\frac{\Gamma\left(\frac{1-m}{m}\right)\Gamma\left(\frac{m+1}{m}\right)}{2^1\left[\Gamma\left(\frac{1}{m}\right)\right]^2} - \mathcal{O}(\delta) + \cdots\right] + \delta^{\frac{1}{m}}\left[\frac{\Gamma\left(\frac{m-1}{m}\right)\Gamma\left(\frac{m+1}{m}\right)}{2^{\frac{1}{m}}\Gamma(1)\Gamma\left(\frac{1}{m}\right)} - \mathcal{O}(\delta) + \cdots\right]. \tag{37} $$

Remembering that $m \geqslant 2$, we see that, as $\delta \to 0^+$, the above is dominated by the term in $\delta^{\frac{1}{m}}$

$$ {}_2F_1\left(\frac{1}{m}, 1; \frac{m+1}{m}; \frac{-1}{\delta}\right) \sim \delta^{\frac{1}{m}}[\mathcal{C}'_0 + \mathcal{C}'_1\delta + \cdots, \tag{38} $$

where the $\{\mathcal{C}'_i\}$ are constants, and $\mathcal{C}'_0 \neq 0$. The behavior around the transition can now be determined:

$$ \lim_{\delta\to 0}\langle D_{\text{eff}}(a = 1+\delta)\rangle_{\text{Sm,P}} = \lim_{\delta\to 0} \delta(2+\delta)(1+\delta)^{-2} D_{\text{free}} \frac{\delta^{-\frac{1}{m}}}{(\mathcal{C}'_0 + \mathcal{C}'_1\delta + \cdots)(\mathcal{C}_0 + \mathcal{C}_1\delta + \cdots)}, $$
$$ \Rightarrow \langle D_{\text{eff}}(a = 1+\delta)\rangle_{\text{Sm,P}} \sim \delta^{1-\frac{1}{m}} \frac{D_{\text{free}}}{\mathcal{C}_0\mathcal{C}'_0} + \mathcal{O}\left(\delta^{2-\frac{1}{m}}\right), \tag{39} $$

as $\delta \to 0^+$. Equation (38) makes clear that the exponent m, which governs the shape of the sections of the energy landscape, determines the behavior around the transition. Sending $m \to \infty$ in Eq. (39) produces a linear dependence upon δ, which, in light of the link between cases 1 and 2 drawn earlier, is as expected.

This analysis makes clear what we noted in case 1: The existence of the transition, and thus the behavior around it, is determined entirely by one of the two integrals in the expression for the averaged effective diffusion coefficient—$\int dQ_1 \langle e^{\beta U_1}\rangle_{\text{x}}\, p(Q_1)$.

B. Cosine energy landscape

The$i$th section $(i = 1, 2, ..., N)$ of the potential energy landscape is defined over the range $[(i-1)L, iL]$ and given by

$$ U_i(x) = \frac{1}{2}Q_i\left[1 - \cos\left(\frac{2\pi x}{L}\right)\right], \tag{40} $$

where the factor of one half is inserted so that the barrier height is Q_i. The first spatial average is

$$ \langle e^{\beta U_1}\rangle_{\text{x}} = \frac{e^{\frac{1}{2}\beta Q_1}}{L}\int_0^L dx\, e^{-\frac{1}{2}\beta Q_1 \cos\left(\frac{2\pi x}{L}\right)}. \tag{41} $$

Hence, the first integral in the expression for the averaged effective diffusion coefficient is

$$ a\beta \int_0^\infty dQ_1 \frac{e^{\frac{1}{2}\beta Q_1}}{L}\int_0^L dx\, e^{-\frac{1}{2}\beta Q_1 \cos\left(\frac{2\pi x}{L}\right)} e^{-a\beta Q_1}. \tag{42} $$

Changing the order of integration and performing the integral over Q_1, we obtain

$$ \int dQ_1 \langle e^{\beta U_1}\rangle_{\text{x}}\, p(Q_1) = \frac{1}{L}\int_0^L dx \frac{2a}{2a - 1 + \cos\left(\frac{2\pi x}{L}\right)}, $$
$$ = \frac{2a}{\sqrt{(2a-1)^2 - 1}}. \tag{43} $$

In the same way, we find the following expression for the second integral:

$$ \int dQ_2 \langle e^{-\beta U_2}\rangle_{\text{x}}\, p(Q_2) = \frac{1}{L}\int_0^L dx \frac{2a}{2a + 1 - \cos\left(\frac{2\pi x}{L}\right)}, $$
$$ = \frac{2a}{\sqrt{(2a+1)^2 - 1}}. \tag{44} $$

Hence, the averaged effective diffusion coefficient is

$$ \langle D_{\text{eff}}\rangle_{\text{C}} = D_{\text{free}} \frac{\sqrt{\left(a - \frac{1}{2}\right)^2 - \frac{1}{4}}\sqrt{\left(a + \frac{1}{2}\right)^2 - \frac{1}{4}}}{a^2}, \tag{45} $$

where the subscript C denotes the case of a cosine energy landscape.

Figure 5 shows the results of Brownian dynamics simulations (performed exactly as before) for a cosine energy landscape; good agreement between simulations results and our theory is observed.

We will now study the properties of the averaged effective diffusion coefficient for the cosine energy landscape. When we send $a \to \infty$ in Eq. (45), the reduction to free diffusion is immediately apparent. Next, we turn our attention to the behavior around the transition point, $a = 1 + \delta$, $\delta \to 0^+$:

$$ \langle D_{\text{eff}}\rangle_{\text{C}} \sim D_{\text{free}}\sqrt{\delta}[1 + \mathcal{O}(\delta)]. \tag{46} $$

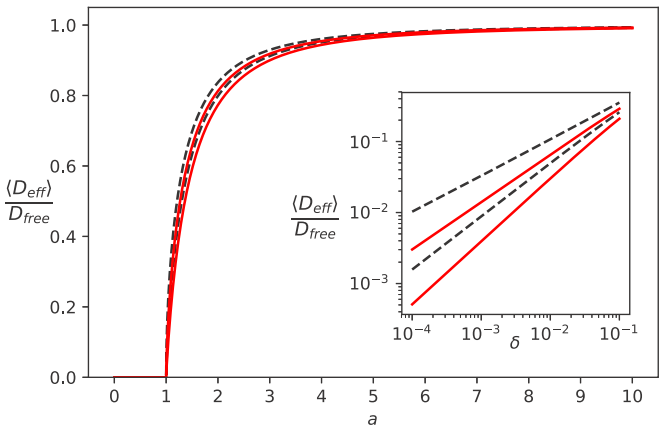

FIG. 4. The averaged effective diffusion coefficient for energy landscapes with smooth maxima characterized by the following powers: $m = 2, 3, 4, 9$ ($m = 2$ is the uppermost line; $m = 9$ is the lowermost). The inset shows the behavior around the transition.

The averaged effective diffusion coefficient behaves as $\delta^{1/2}$, which is an interesting result when viewed in the context of previous work on "power law forms." Equation (39) tells us that when $m = 2$ (quadratic energy landscape), the averaged affective diffusion coefficient also behaves as $\delta^{1/2}$. Expanding each of the energy landscapes around its maxima:

$$U_{i,m=2} = Q_i\left[1 - \left(\frac{2\delta x}{L}\right)^2\right], \tag{47}$$

$$U_{i,\text{cosine}} = \frac{Q_i}{2}\left[2 - \frac{1}{2!}\left(\frac{2\pi\delta x}{L}\right)^2 + \cdots\right], \tag{48}$$

we see that the order of the first nonvanishing derivative (second) is the same. In the next subsection, we will demonstrate that the behavior of the averaged effective diffusion coefficient around the transition is determined by the order of the first nonvanishing derivative in the series expansion of the potential energy landscape around its maxima.

It is evident from Figs. 3, 4, and 5 that, irrespective of the value of m, the averaged effective diffusion coefficient

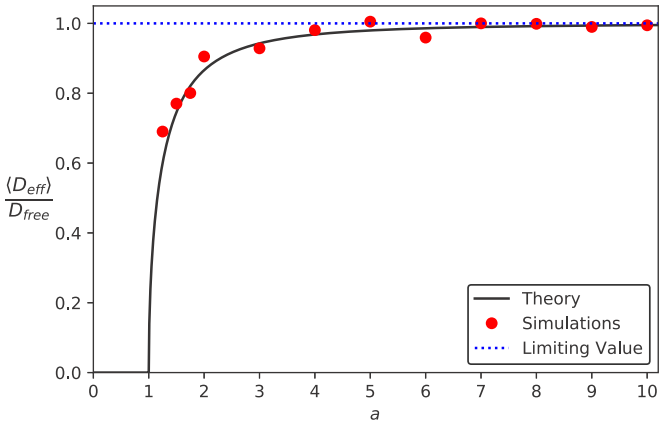

FIG. 5. The results of Brownian dynamics simulations (red circles) are presented alongside the theoretical prediction (solid line) for the cosine energy landscape.

saturates quickly to the free diffusive limit. This reinforces the notion that the most interesting behavior occurs in the region around the transition.

C. Generalization for smooth maxima

As remarked before, the relevant integral is $\int dQ_1 \langle e^{\beta U_1}\rangle_x\, p(Q_1)$. Our approach is similar to the saddle-point approximation used by Kramers [31].

1. Symmetric maxima

Consider a piecewise-defined potential energy landscape $U(x)$ where each section has the same general form; only the height of the central, symmetric maximum differs from one section to the next. Expanding $U_1(x)$ about its maximum, we obtain $U_1(x) \approx Q_1 - \frac{1}{m!}|U^{(m)}(\frac{L}{2})||x - \frac{L}{2}|^m$, where m is the order of the first nonvanishing derivative, and modulus signs have been used both to introduce a minus sign and to account for piecewise defined maxima characterized by odd exponents. Rewriting $U^{(m)}(\frac{L}{2}) = Q_1 V^{(m)}(\frac{L}{2})$, the relevant integral is given approximately by

$$\frac{a\beta}{L}\int_0^\infty dQ_1 \int_0^L dx\, e^{\beta Q_1} e^{-\frac{1}{m!}|V^{(m)}(\frac{L}{2})||x-\frac{L}{2}|^m} e^{-a\beta Q_1}. \tag{49}$$

Swapping the order of integration, evaluating the integral over Q_1, and exploiting the symmetry about $x = L/2$, we obtain

$$\frac{2a}{L}\int_{\frac{L}{2}}^L dx \frac{1}{(a-1) + \frac{1}{m!}\left(\frac{L}{2}\right)^m \left|V^{(m)}\left(\frac{L}{2}\right)\right|\left(\frac{2x}{L} - 1\right)^m}. \tag{50}$$

Changing variables to $u = \frac{2x}{L} - 1$ and dividing through to eliminate its prefactor $c = \frac{1}{m!}|V^{(m)}(\frac{L}{2})|$, we find

$$\int dQ_1 \langle e^{\beta U_1}\rangle_x\, p(Q_1) \approx \frac{a}{a-1}\,{}_2F_1\left(\frac{1}{m}, 1; 1 + \frac{1}{m}; \frac{-c}{a-1}\right). \tag{51}$$

As before, the behavior around the transition is determined by setting $a = 1 + \delta$ and examining the limiting form as $\delta \to 0^+$. From Eq. (38), we deduce

$$\frac{1+\delta}{\delta}\,{}_2F_1\left(\frac{1}{m}, 1; 1 + \frac{1}{m}; \frac{-c}{\delta}\right) \sim \frac{(1+\delta)}{\delta^{1-\frac{1}{m}}}[\mathcal{C}_0' + \mathcal{C}_1'\delta + \cdots]. \tag{52}$$

Since the averaged effective diffusion coefficient is inversely proportional to the above, we find

$$\langle D_{\text{eff}}\rangle \sim \delta^{1-\frac{1}{m}} \frac{D_{\text{free}}}{\mathcal{C}_0\mathcal{C}_0'}, \tag{53}$$

where $\mathcal{C}_0$ is a constant arising from the other integral in the full expression for D_{eff}. Hence, the link between the curvature of the potential energy landscape around its maxima and the behavior of the averaged effective diffusion coefficient around the transition point is clear.

2. Asymmetric maxima

Suppose instead that the maxima are asymmetric. Then, in order to evaluate the relevant integral, we must expand the potential energy landscape on both sides of the maximum.

Denoting the expansion to the left- and right-hand sides by $U_{\mathcal{L}}$ and $U_{\mathcal{R}}$, respectively, we have

$$U_{1,\mathcal{L},\mathcal{R}} = Q_1\left[1 - \frac{1}{m_{\mathcal{L},\mathcal{R}}!}\left|V^{m_{\mathcal{L},\mathcal{R}}}\left(\frac{L}{2}\right)\right|\left|x - \frac{L}{2}\right|^{m_{\mathcal{L},\mathcal{R}}}\right], \quad (54)$$

Proceeding as in the previous case and evaluating the integral over Q_1, we obtain

$$\frac{a}{L}\sum_{i=\mathcal{L},\mathcal{R}}\int_{\frac{L}{2}}^{L}\frac{dx}{(a-1) + \frac{1}{m_i!}\left(\frac{L}{2}\right)^{m_i}\left|V^{m_i}\left(\frac{L}{2}\right)\right|\left(\frac{2x}{L} - 1\right)^m}, \quad (55)$$

where we have used the symmetry of $U_{1,\mathcal{L}}$ about $x = L/2$ to define both integrals over the same spatial range. From results established when studying symmetric maxima, the above evaluates to

$$\frac{a}{2(a-1)}\sum_{i=\mathcal{L},\mathcal{R}} {}_2F_1\left(\frac{1}{m_i}, 1; 1 + \frac{1}{m_i}; \frac{-c_i}{a-1}\right). \quad (56)$$

The behavior of the averaged effective diffusion coefficient around the transition point is then easily found:

$$\langle D_{\text{eff}}\rangle \sim \frac{\delta}{\mathcal{C}_{\mathcal{L}}\delta^{\frac{1}{m_{\mathcal{L}}}} + \mathcal{C}_{\mathcal{R}}\delta^{\frac{1}{m_{\mathcal{R}}}}}, \quad (57)$$

where $\mathcal{C}_{\mathcal{L},\mathcal{R}}$ are constants. The denominator of the above is dominated by the term with the smallest exponent, i.e., by the larger of $m_{\mathcal{L}}$ and $m_{\mathcal{R}}$.

This concludes the proof and demonstrates wider applicability than the simplest case of symmetric maxima.

D. Example: Random powers *m*

To build upon ideas laid out above and to illustrate their broad applicability, we will study the case of piecewise-defined potential energy landscapes where the constituent sections need no longer have the same shape. A probability distribution is assigned to m and the expression for the averaged effective diffusion coefficient [Eq. (20)] is modified accordingly:

$$\langle D_{\text{eff}}\rangle_{\text{R}} = \frac{D_{\text{free}}}{\int dm_1\left[\int dQ_1 \langle e^{\beta U_1}\rangle_{\text{x}}\, p_Q(Q_1)\right]p_m(m_1)} \times \frac{1}{\int dm_2\left[\int dQ_2 \langle e^{-\beta U_2}\rangle_{\text{x}}\, p_Q(Q_2)\right]p_m(m_2)}, \quad (58)$$

where R denotes the case of "random powers" and p_m and p_Q denote the probability distributions for shape and amplitude, respectively.

Working with the energy landscape given at the start of "power law forms," $U_i(x) = Q_i(1 - [\frac{2x}{L} - (2i-1)]^m)$, the averaged effective diffusion coefficient is

$$\langle D_{\text{eff}}\rangle_{\text{R}} = \frac{\left(1 - \frac{1}{a^2}\right)D_{\text{free}}}{\int dm_1\left[{}_2F_1\left(\frac{1}{m_1}, 1; \frac{m_1+1}{m_1}; \frac{-1}{a-1}\right)\right]p_m(m_1)} \times \frac{1}{\int dm_2\left[{}_2F_1\left(\frac{1}{m_2}, 1; \frac{m_2+1}{m_2}; \frac{1}{a+1}\right)\right]p_m(m_2)}. \quad (59)$$

By way of example, we choose a δ-function distribution for m: $p_m(m) = \sum_i \alpha_i \delta(m - m_i)$, where $\sum_i \alpha_i = 1$ ensures normalization. In Eq. (59), we find

$$\langle D_{\text{eff}}\rangle_{\text{R}} = \frac{\left(1 - \frac{1}{a^2}\right)D_{\text{free}}}{\sum_i \alpha_i\left[{}_2F_1\left(\frac{1}{m_i}, 1; \frac{m_i+1}{m_i}; \frac{-1}{a-1}\right)\right]} \times \frac{1}{\sum_j \alpha_j\left[{}_2F_1\left(\frac{1}{m_j}, 1; \frac{m_j+1}{m_j}; \frac{1}{a+1}\right)\right]}. \quad (60)$$

Note that we have assumed that there are only a finite number of different powers m_i. As $a \to \infty$, the usual reduction to free diffusion takes place. In a manner similar to the one before, the expression for the averaged effective diffusion coefficient around the transition point (as $\delta \to 0^+$)

$$\langle D_{\text{eff}}(a = 1 + \delta)\rangle_{\text{R}} \sim D_{\text{free}}\frac{\delta}{\sum_i \alpha_i \mathcal{C}'_{i,0}\delta^{\frac{1}{m_i}}\sum_j \alpha_j \mathcal{C}_{j,0}}. \quad (61)$$

The denominator of the above will be dominated by the term with the largest value of m, which we shall denote by $m_{\max}$. Hence, we find

$$\langle D_{\text{eff}}(a = 1 + \delta)\rangle_{\text{R}} \sim \frac{D_{\text{free}}\delta^{1 - \frac{1}{m_{\max}}}}{\mathcal{C}}, \quad (62)$$

where $\mathcal{C}$ is a constant. Larger values of m correspond to flatter energy landscapes, so the behavior around the transition is determined by the flattest section of the energy landscape.

The behavior for other probability distributions p_m is harder to determine analytically.

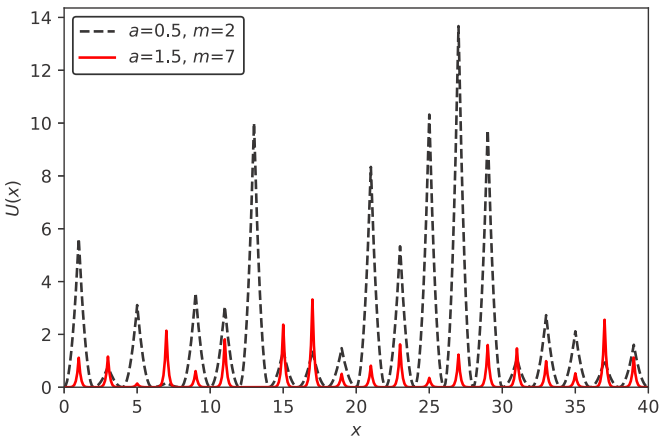

FIG. 6. Example energy landscapes with sharp maxima: The black (dashed) and red (solid) lines correspond to $a = 0.5$, $m = 2$ and $a = 1.5$, $m = 7$, respectively ($L = 2$).

V. CASE 3: SHARP MAXIMA

The ith section ($i = 1, 2, ..., N$) of the potential energy landscape is defined over the range $[(i-1)L, iL]$ in a piecewise manner. The first half from $x = (i-1)L$ to $x = (i - \frac{1}{2})L$ (i.e., from $U = 0$ to $U = Q_i$) is given by

$$U_i(x) = Q_i\left[\frac{2x}{L} - (i-1)\right]^m, \quad (63)$$

where $m \geqslant 2$. The second half is the mirror image in the line $x = (i - \frac{1}{2})L$. An example is shown in Figure 6. We will employ the same methodology as in the case of smooth

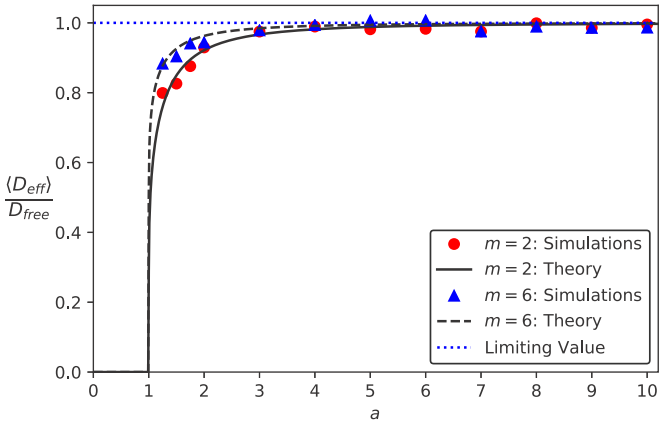

FIG. 7. The results of Brownian dynamics simulations (red circles and blue triangles) are presented alongside the theoretical predictions (solid and dashed lines) for two energy landscapes characterized by $m = 2$, and $m = 6$, respectively.

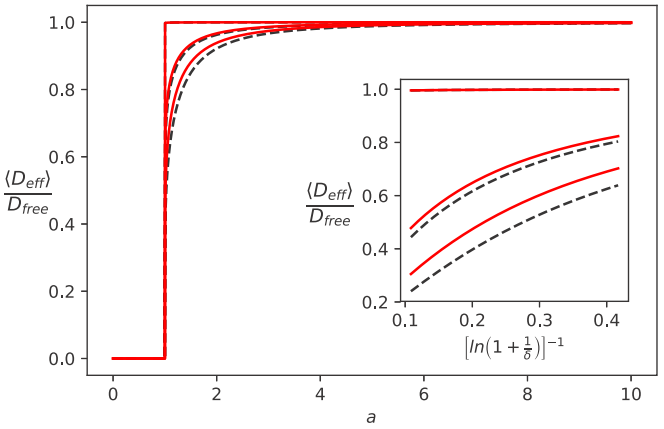

FIG. 8. The averaged effective diffusion coefficient for energy landscapes with sharp maxima characterized by the following powers: $m = 2, 3, 6, 7, 2000, 2001$ ($m = 2$ is the lowermost line; $m = 2001$ the uppermost). The inset shows the region around the transition point ($\delta = 10^{-4}$ to 10^{-1}), and highlights the linear behavior for small values of δ.

maxima to derive the averaged effective diffusion coefficient. The integrals in the expression for the averaged effective diffusion coefficient are

$$\frac{2a\beta}{L}\int_0^\infty dQ_1 \int_0^{L/2} dx\, e^{-[a-(\frac{2x}{L})^m]\beta Q_1}, \quad \frac{2a\beta}{L}\int_0^\infty dQ_2 \int_0^{L/2} dx\, e^{-[a+(\frac{2x}{L})^m]\beta Q_2}, \tag{64}$$

where the factors of 2 come from exploiting the symmetry of the integrand about the maxima. Swapping the order of integration and changing variable enables us to write the averaged effective diffusion coefficient as

$$\langle D_{\rm eff}\rangle_{\rm Sh} = \frac{D_{\rm free}}{a^2 \int_0^1 du \frac{1}{a-u^m}\int_0^1 dv \frac{1}{a+v^m}}, \tag{65}$$

where the subscript "Sh" denotes the case of "sharp maxima." Finally, evaluating these integrals in terms of hypergeometric functions, we find

$$\langle D_{\rm eff}\rangle_{\rm Sh} = \frac{D_{\rm free}}{{}_2F_1\left(\frac{1}{m}, 1; \frac{m+1}{m}; \frac{1}{a}\right){}_2F_1\left(\frac{1}{m}, 1; \frac{m+1}{m}; -\frac{1}{a}\right)}. \tag{66}$$

Note that as $a \to \infty$ the system returns to free diffusion. Figure 7 shows the results of Brownian dynamics simulations for two energy landscapes with sharp maxima. Good agreement between the simulations and our theory is observed.

As in the case of smooth maxima, the averaged effective diffusion coefficient saturates quickly to the free diffusive limit. In fact, the saturation takes place more rapidly for sharp maxima. This can be seen in Fig. 8.

Setting $a = 1 + \delta$ in Eq. (66), the averaged effective diffusion coefficient becomes

$$\langle D_{\rm eff}\rangle_{\rm Sh} = \frac{D_{\rm free}}{{}_2F_1\left(\frac{1}{m}, 1; \frac{m+1}{m}; \frac{-1}{1+\delta}\right){}_2F_1\left(\frac{1}{m}, 1; \frac{m+1}{m}; \frac{1}{1+\delta}\right)}. \tag{67}$$

The first of the above hypergeometric functions—${}_2F_1(\frac{1}{m}, 1, \frac{m+1}{m}; \frac{-1}{1+\delta})$—is equal to some constant $\mathcal{C}_0$ for $\delta = 0$; it does not contribute to the leading-order behavior around the transition.

Turning to the second hypergeometric function, it is possible to show that, as $\delta \to 0$, it becomes

$$\frac{1}{m}\left[\ln\left(1+\frac{1}{\delta}\right) - \psi^{(0)}\left(\frac{1}{m}\right) - \gamma\right][1 + \mathcal{O}(\delta)], \tag{68}$$

where $\psi^{(0)}(x) = \frac{d}{dx}\ln(\Gamma(x))$ is the Digamma function and γ is the Euler-Mascheroni constant [30]. As $\delta \to 0$, the logarithm diverges towards plus infinity. Clearly, therefore, the behavior of the averaged effective diffusion coefficient around the transition point is considerably stronger than in the case of smooth maxima. Furthermore, as $m \to \infty$, $-\frac{1}{m}\psi^{(0)}(\frac{1}{m}) \to \infty$. Therefore, energy landscapes with sharper maxima will be characterized by averaged effective diffusion coefficients that display a steeper behavior around the transition.

Inserting these limiting forms into Eq. (67), we find

$$\langle D_{\rm eff}\rangle_{\rm Sh} \sim \frac{mD_{\rm free}}{\mathcal{C}_0\left[\ln\left(1+\frac{1}{\delta}\right) - \psi^{(0)}\left(\frac{1}{m}\right) - \gamma\right]}. \tag{69}$$

This behavior around the transition—$[\ln(1/\delta)]^{-1}$ at the weakest—stands in stark contrast to the power-law dependencies observed for smooth maxima: $\delta^{\frac{1}{2}}$ to δ^1 (for $m = 2$ and $m \to \infty$, respectively).

VI. SUBDIFFUSION

The averaged effective diffusion coefficient—Eq. (20)– -is only nonzero for values of $a > 1$. When $a \leqslant 1$, one of the integrals in the denominator diverges, indicating a change in the system's behavior from diffusive to subdiffusive.

The random barrier and random trap models offer a framework to study the subdiffusive regime. The former considers the hopping motion of particles over potential energy barriers and is characterized by transition rates; the latter considers the escape from potential energy minima and is characterized by trapping times. In one dimension, provided that one identifies the reciprocal of the transition rates with the mean trapping time, then the models predict identical behavior [16].

By assuming a simple exponential relationship between barrier height (trap depth) Q and mean first-passage (trapping) time τ, $\tau = \tau_0 \exp(\beta Q)$, and the usual exponential distribution of barrier heights (trap depths) across lattice sites, $p(Q) = a\beta \exp(-a\beta Q)$, the distribution of mean first-passage (trapping) times can be calculated:

$$\psi(\tau) = \frac{p(Q)}{d\tau/dQ} = \frac{a\tau_0^a}{\tau^{1+a}}. \tag{70}$$

Consequently, the evolution of the mean squared displacement can be derived:

$$\begin{aligned} a < 1 &: \langle x^2(t)\rangle \sim t^{2\nu}, \\ a = 1 &: \langle x^2(t)\rangle \sim t/\ln(t), \end{aligned} \tag{71}$$

where $\nu = a/(1+a)$ [13,15,16].

In this work, rather than specifying the relationship between the barrier height and the mean first-passage time, we specify the form of the potential energy barrier and subsequently derive the mean first-passage time. For the energy barriers considered in this work, the double-integral expression for the mean first-passage time cannot be evaluated analytically. As such, the above expressions for the distribution of mean first-passage time and the mean squared displacement are *not* expected to hold true. Nonetheless, it is instructive to compare their predictions with the results of numerical simulations. We will consider the distribution of mean first-passage times, before studying the evolution of the mean squared displacement.

A. Distribution of mean first-passage times $\psi(\tau)$

For $U(x) = Q[1 - |\frac{2x}{L}|^m]$, the mean first-passage time from $x = -\frac{L}{2}$ to $x = \frac{L}{2}$ is [22]

$$\tau = \frac{L^2}{4D}\int_{-1}^{1} du\, e^{-\beta Q|u|^m} \int_{-1}^{u} dv\, e^{\beta Q|v|^m}. \tag{72}$$

The distribution of mean first-passage times is calculated as before: Differentiating Eq. (72), we find that

$$\begin{aligned} \psi = \frac{2Dm}{L^2} a\beta Q e^{-a\beta Q}\Bigg[e^{\beta Q}\int_0^1 du\, e^{-\beta Q u^m} + e^{-\beta Q}\int_0^1 du\, e^{\beta Q u^m} \\ - \int_{-1}^{1} du\, e^{-\beta Q|u|^m}\int_{-1}^{u} dv\, e^{\beta Q|v|^m}\Bigg]^{-1}. \end{aligned} \tag{73}$$

Unlike the random barrier (trap) model, where the mean first-passage time is a simple exponential, the derivative $d\tau/dQ$ cannot be expressed in terms of τ alone. Consequently, the distribution ψ is not a power law, though it is well approximated as such for values of $\beta Q \gtrsim 1$. In fact, for a given value of a, as βQ increases, the characteristic exponent approaches the βQ-independent value of $1 + a$. For tall barriers (large βQ), the mean first-passage time is approximately

$$\tau \approx \frac{L^2}{2D}\frac{\Gamma\left(\frac{1}{m}\right)e^{\beta Q}}{m(\beta Q)^{1+\frac{1}{m}}}, \tag{74}$$

while the distribution of mean first-passage times is

$$\psi \approx \frac{2D}{L^2}\frac{am^2}{\Gamma\left(\frac{1}{m}\right)}\frac{(\beta Q)^{1+\frac{1}{m}}}{e^{(1+a)\beta Q}}. \tag{75}$$

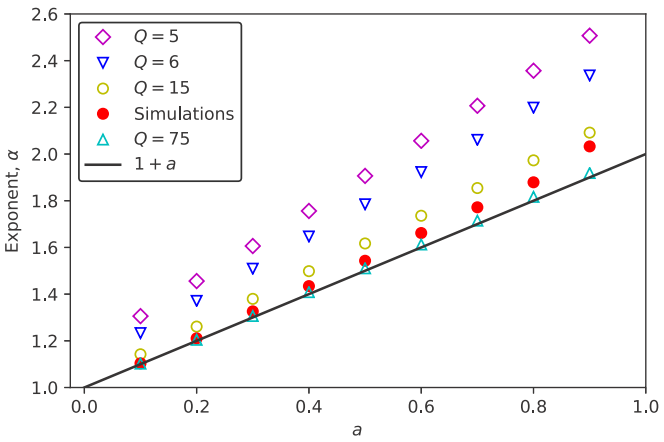

FIG. 9. The power-law exponent α is calculated for different amplitudes Q over a range of values of a for a quadratic maximum ($m = 2$). The results of numerical simulations are also shown for comparison.

Studying the limiting form of the natural logarithm of Eqs. (74) and (75), it is possible to establish the following, approximate, relationship,

$$\ln\psi \sim -(1+a)\ln\tau + \text{const.}, \tag{76}$$

which confirms that, in the large-amplitude limit, the distribution of mean first-passage times obeys the power law predicted by the random barrier model.

In order to test this prediction, we simulated as follows using unit values of thermal energy and damping throughout: For a given value of a, the distribution of barrier heights $p(Q)$ was sampled until 10^5 values of Q larger than some large threshold value (we used $Q_T = 15$) were obtained. The corresponding mean first-passage times over the quadratic ($m = 2$) maximum were calculated [22], their distribution analyzed, and the characteristic exponent, α, extracted [32]. A threshold was used because large amplitudes are less probable than small amplitudes, but more important in determining the exact behavior of the distribution's heavy tail.

Figure 10 shows the results of these numerical simulations. Also presented are the results of a separate analysis of the behavior of the distribution of mean first-passage times: Using Eqs. (72) and (73), it is possible to calculate the characteristic power-law exponent α for a given value of Q, over a range of values of a.

Figure 9 demonstrates that, for a given value of a, as the value of Q at which the exponent α is calculated is increased, the deviation from the random barrier model's prediction decreases, so lending support to Eq. (76).

Choosing a constant threshold for Q affects the simulation results: The probability of obtaining a value of Q larger than a threshold Q_T is $e^{-a\beta Q_T}$. For unit thermal energy and $Q_T = 15$, these probabilities are 0.22 and 1.4×10^{-6} for $a = 0.1$ and $a = 0.9$, respectively. This means that the barrier heights, and hence the mean first-passage times, obtained for $a = 0.1$ will be distributed over a large range, thus allowing the characteristic exponent to be calculated accurately. By contrast, the barrier heights obtained for $a = 0.9$ will be relatively tightly distributed above the threshold, so giving rise

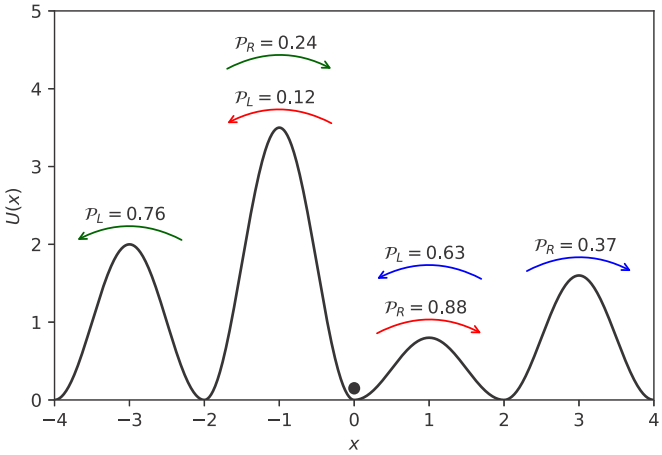

FIG. 10. The hopping probabilities for a section of an example energy landscape are calculated according to Eq. (69). The particles make transitions based upon these probabilities and a mean first-passage time calculated for each minimum.

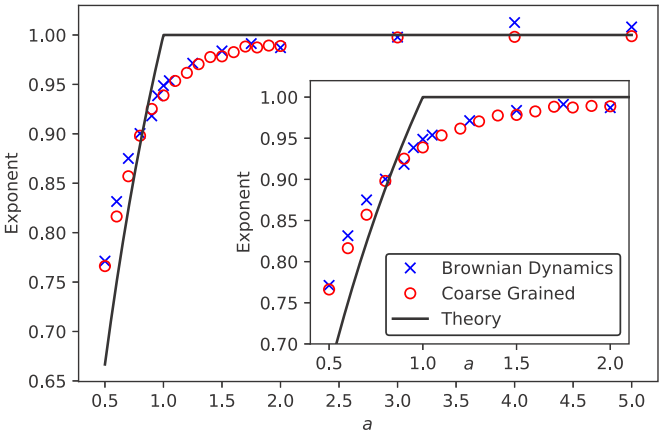

FIG. 11. The exponents characterizing the growth of the mean squared displacement with time extracted from Brownian dynamics (BD) and coarse-grained simulations are plotted as a function of a. The inset is an enlargement of the region around $a = 1$.

to a characteristic exponent greater than that predicted by the random barrier model.

Increasing the number of samples would, eventually, undoubtedly produce a characteristic exponent very close to the value predicted by the random barrier model: Figure 9 indicates that good agreement is observed for $Q \sim 75$, which, for $a = 0.9$, has a probability of occurrence of roughly 5×10^{-30}. Were a Brownian particle to move in such a landscape it is clear that the mean time elapsed before encountering a barrier of this height would be vast. Hence, we believe that the subdiffusive dynamics differ from the random barrier model's predictions on possibly substantial timescales.

B. Evolution of the mean squared displacement

In order to investigate the behavior of the mean squared displacement, we performed two types of numerical simulations.

The first were Brownian dynamics simulations: An ensemble of particles was initialized at $x = 0$ in a piecewise-defined cosine energy landscape, where the amplitude of each section was obtained from the exponential distribution $p(Q) = a\beta \exp(-a\beta Q)$. With unit values of thermal energy and damping, the system evolved until the mean squared displacement was at least $1000L^2$. For a given value of a, this procedure was repeated for 500 energy landscapes, with ten particles per landscape. After combining the trajectories $\langle x^2(t)\rangle$, the exponent 2ν was extracted.

The second was a coarse-grained version of the above. Instead of advancing the position of each particle according to a simulation scheme based upon the overdamped Langevin equation, we constructed a scheme based upon the random barrier model: The minima were regarded as lattice sites, between which particles could hop. Consider the following part of an energy landscape:

$$U(x) = \begin{cases} Q_1\left[1 - \cos\left(\frac{2\pi x}{L}\right)\right], & -L \leqslant x \leqslant 0, \\ Q_2\left[1 - \cos\left(\frac{2\pi x}{L}\right)\right], & 0 \leqslant x \leqslant L. \end{cases}$$

For a particle starting from $x = 0$, the probabilities of exiting the region $[-L, L]$ to the left, and to the right, are given by [22]

$$\begin{aligned} \mathcal{P}_L &= \frac{\int_0^L dx\, e^{\beta U}}{\int_{-L}^L dx\, e^{\beta U}} = \frac{e^{\beta Q_2} I_0(\beta Q_2)}{e^{\beta Q_1} I_0(\beta Q_1) + e^{\beta Q_2} I_0(\beta Q_2)}, \\ \mathcal{P}_R &= \frac{\int_{-L}^0 dx\, e^{\beta U}}{\int_{-L}^L dx\, e^{\beta U}} = \frac{e^{\beta Q_1} I_0(\beta Q_1)}{e^{\beta Q_1} I_0(\beta Q_1) + e^{\beta Q_2} I_0(\beta Q_2)}, \end{aligned} \tag{77}$$

respectively, while the mean first-passage time to move from the central minimum to either of the adjacent minima is [22]

$$\tau = \mathcal{P}_R \int_0^L dy\, e^{\beta U} \int_{-L}^y dz\, e^{-\beta U} - \mathcal{P}_L \int_{-L}^0 dy\, e^{\beta U} \int_{-L}^y dz\, e^{-\beta U}. \tag{78}$$

Figure 10 illustrates the hopping process laid out above. In particular, it makes clear that the same energy barrier has different probabilities of being crossed depending upon the direction in which the particle is moving.

Simulations were carried out as follows: 10^3 particles were initialized at $x = 0$ in a piecewise-defined cosine energy landscape $U_i(x) = \frac{Q_i}{2}[1 - \cos(n\pi x)]$, where the amplitude of each section was taken from the usual exponential distribution. Each particle made 500 jumps, with the direction of each jump determined in accordance with the probabilities given above. The time associated with each jump was taken from an exponential distribution whose mean was the above mean first-passage time [15]. This process was repeated for 10^3 energy landscapes, and the resulting trajectories used to calculate the evolution of the mean squared displacement with time. The exponent 2ν was then extracted.

We decided to use this coarse-grained simulation scheme because it is much faster than conventional Brownian dynamics simulations. That it cannot replicate the short-time behavior as the ensemble spreads out within a single minimum before particles make their first transition is unimportant, because we are interested only in the long-time, interwell behavior.

Figure 11 shows the results of both types of simulations, and the random barrier model's prediction.

Good agreement between the results of Brownian dynamics simulations and coarse-grained simulations is observed. However, significant disagreement with both the random barrier model's and Eq. (20)'s predictions is also apparent: The sharp transition from subdiffusion to diffusion at $a = 1$ is not borne out by the simulations. Rather, a gradual change occurs, with subdiffusive behavior persisting well into the (predicted) diffusive regime. We do not have a concrete explanation for this observation. However, we believe that it is possible that the system's behavior is transient, becoming diffusive only at very long times, beyond those for which motion was simulated.

VII. CONCLUSIONS

In this paper, we used the concept of an *averaged* effective diffusion coefficient $\langle D_{\text{eff}} \rangle$ to build upon work done by Banerjee *et al.* and Zwanzig. The (one-dimensional) mean first-passage time formalism was used to derive an expression for $\langle D_{\text{eff}} \rangle$ in terms of the piecewise-defined energy landscape $U(x)$ and the probability distribution $p(Q)$ from which the amplitudes of each section of the landscape were taken. We calculated the averaged effective diffusion coefficient for an exponential probability distribution $p(Q) = a\beta \exp(-a\beta Q)$ for energy landscapes characterized by flat sections, smooth maxima, and sharp maxima. In every case, a transition from subdiffusive to diffusive behavior was observed at $a = 1$. The behavior of $\langle D_{\text{eff}} \rangle$ around the transition was found to depend heavily upon the nature of $U(x)$. For energy landscapes with smooth maxima, $\langle D_{\text{eff}} \rangle$ scales as $(a-1)^{1-\frac{1}{m}}$, where $m \geqslant 2$ is the order of the first nonvanishing derivative of $U(x)$ evaluated at its maxima. Conversely, energy landscapes with sharp maxima displayed strongly divergent, nonanalytical behavior around the transition; the sharper the energy landscape, the stronger the divergence. We also studied two aspects of the subdiffusive ($a < 1$) regime: the growth of the mean squared displacement with time $\langle x^2(t) \rangle$ and the distribution of mean first-passage times $\psi(\tau)$. The shapes of the maxima here considered resulted in a nonanalytic expression for the mean first-passage time. As a direct consequence, predictions made within the framework of the random barrier model, where $\tau \sim \exp(\beta Q)$, were no longer expected to be accurate. Correspondingly, only limited agreement was found between the exponent characterizing subdiffusion obtained from Brownian dynamics simulations and that predicted by the random barrier model. Additionally, the distribution of mean first-passage times was found no longer to be a power law. However, in the limit of large barriers, a reduction to power-law behavior—with the same characteristic exponent as that predicted by the random barrier model—is observed.

ACKNOWLEDGMENTS

T.H.G. acknowledges support from the EPSRC and E.H.Y. acknowledges support from Nanyang Technological University, Singapore, under Grant No. M4081583.

[1] A. Einstein, Ann. Phys. **17**, 549 (1905).
[2] M. von Smoluchowski, Ann. Phys. **326**, 756 (1906).
[3] A. Morin, D. Lopes Cardozo, V. Chikkadi, and D. Bartolo, Phys. Rev. E **96**, 042611 (2017).
[4] T. V. Ratto and M. L. Longo, Langmuir **19**, 1788 (2003).
[5] P. Tan, Y. Liang, Q. Xu, E. Mamontov, J. Li, X. Xing, and L. Hong, Phys. Rev. Lett. **120**, 248101 (2018).
[6] U. Choudhury, A. V. Straube, P. Fischer, J. G. Gibbs, and F. Höfling, New J. Phys. **19**, 125010 (2017).
[7] Y. Su, P.-Y. Lai, B. J. Ackerson, X. Cao, Y. Han, and P. Tong, J. Chem. Phys. **146**, 214903 (2017).
[8] C. Emary, R. Gernert, and S. H. L. Klapp, Phys. Rev. E **86**, 061135 (2012).
[9] X.-g. Ma, P.-Y. Lai, and P. Tong, Soft Matter **9**, 8826 (2013).
[10] F. Evers, C. Zunke, R. D. L. Hanes, J. Bewerunge, I. Ladadwa, A. Heuer, and S. U. Egelhaaf, Phys. Rev. E **88**, 022125 (2013).
[11] Y. Su, X.-g. Ma, P.-Y. Lai, and P. Tong, Soft Matter **13**, 4773 (2017).
[12] Y. A. Berlin and A. L. Burin, Chem. Phys. Lett. **257**, 665 (1996).
[13] S. Alexander, J. Bernasconi, W. R. Schneider, and R. Orbach, Rev. Mod. Phys. **53**, 175 (1981).
[14] C. Monthus and J.-P. Bouchaud, J. Phys. A: Math. Gen. **29**, 3847 (1996).
[15] E. M. Bertin and J.-P. Bouchaud, Phys. Rev. E **67**, 026128 (2003).
[16] J.-P. Bouchaud and A. Georges, Phys. Rep. **195**, 127 (1990).
[17] R. Salgado-Garca, Phys. A (Amsterdam, Neth.) **453**, 55 (2016).
[18] P. Hänggi, P. Talkner, and M. Borkovec, Rev. Mod. Phys. **62**, 251 (1990).
[19] S. Lifson and J. L. Jackson, J. Chem. Phys. **36**, 2410 (1962).
[20] J. L. Jackson and S. R. Coriell, J. Chem. Phys. **38**, 959 (1963).
[21] R. Zwanzig, Proc. Natl. Acad. Sci. USA **85**, 2029 (1988).
[22] C. Gardiner, *Handbook of Stochastic Methods for Physics, Chemistry, and the Natural Sciences*, Springer Complexity Series (Springer, Berlin, 2004).
[23] S. Banerjee, R. Biswas, K. Seki, and B. Bagchi, J. Chem. Phys. **141**, 124105 (2014).
[24] J. P. Bouchaud, J. Phys. I France **2**, 1705 (1992).
[25] G. B. Arous, A. Bovier, and V. Gayrard, Phys. Rev. Lett. **88**, 087201 (2002).
[26] B. Derrida, J. Stat. Phys. **31**, 433 (1983).
[27] R. Zwanzig, J. Stat. Phys. **28**, 127 (1982).
[28] J. Haus and K. Kehr, Phys. Rep. **150**, 263 (1987).
[29] J. R. Kalnin and A. M. Berezhkovskii, J. Chem. Phys. **139**, 196101 (2013).
[30] M. Abramowitz and I. A. Stegun, *Handbook of Mathematical Functions with Formulas, Graphs, and Mathematical Tables* (Dover, New York, 1964).
[31] H. Kramers, Phys. (Amsterdam, Neth.) **7**, 284 (1940).
[32] J. Alstott, E. Bullmore, and D. Plenz, PLoS ONE **9**, e95816 (2014).

Correction: A footnote indicating the corresponding author's email address has been inserted.